Continental Shelf Research, Vol. 5, No. 6, pp. 611 to 628, 1986.
Printed in Great Britain.

0278-4343/86 $3.00 + 0.00

Tidal-induced buoyancy flux and mean transverse circulation

HSIEN WANG OU* and LEO MAAS†

(*Received* 27 *September* 1984; *in revised form* 21 *May* 1985; *accepted* 30 *May* 1985)

Abstract—A weakly nonlinear model is used to examine the mean transverse circulation (cross-isobath) driven by tidal-induced buoyancy flux. The mean Eulerian flows driven by both the barotropic and baroclinic tide are presented for a semi-infinite wedge. The mean flow driven by the barotropic tide is significant only near the apex where the thickness of the frictional boundary layer is comparable to the water depth. The mean flow there is characterized by a single-cell circulation with offshore flow near the bottom, and its magnitude can reach a few percentage or a significant fraction of the tidal velocity in oceanic applications. The mean flow driven by the baroclinic tide, on the other hand, is characterized by pairs of half-open (on the seaward side) counter-rotating cells, the number of which equals the vertical mode number. For a baroclinic tide propagating onshore, the mean flow near the top and bottom surfaces is always directed offshore and its magnitude can reach a large fraction of the tidal velocity. Taken together, the model thus predicts a mean offshore flow near the bottom while higher up in the water column the mean flow direction is less definite due to the contribution from different tidal components. The model results are consistent with some current measurements over the Georges Bank.

1. INTRODUCTION

IN MOST studies of the tidal rectification (e.g. ZIMMERMAN, 1980; LODER, 1980), the nonlinear momentum transfer is provided by the Reynolds stress, the spatial inhomogeneity of which drives the residual flow. In a stratified ocean, the tides can also generate a buoyancy flux and conceivably the spatial inhomogeneity of this flux can induce a mean vertical motion and, through mass continuity and kinematic boundary constraint, a mean circulation. For a shelf geometry that is uniform in the alongshelf direction, this circulation occurs on a plane perpendicular to the isobaths and hence will be referred to as the transverse circulation.

The concept of a mean flow driven by buoyancy fluxes is not new, and has been explored to some extent in the context of internal waves (e.g. CHARNEY and DRAZIN, 1961; BRETHERTON, 1969; WUNSCH, 1971; MCINTYRE, 1977). We will however apply the theory specifically to the tidal problem and to address two practical questions: What is the structure of the mean transverse circulation? And what is its magnitude?

Since under the present mechanism, the transverse circulation is driven solely by the buoyancy flux, it is independent of the momentum balance. On the other hand, the Coriolis force acting on this transverse circulation provides a source term in the alongshelf

This paper was presented at the symposium on "Topographic Interactions and Residual Currents" in Texel, The Netherlands on 3 to 4 May, 1984.

* Lamont-Doherty Geological Observatory of Columbia University, Palisades, NY 10964, U.S.A.
† Institute of Meteorology and Oceanography, University of Utrecht, Princetonplein 5, Utrecht 2506, The Netherlands.

momentum balance and can drive a residual flow along isobaths. Not certain about the structure and the magnitude of this circulation, researchers in the past have frequently neglected this Coriolis term in the mean momentum balance, sometimes without sufficient justification. The model results would enable some assessment of this term and in particular its effect on the vertical structure of the residual flow along isobaths.

The problem we are considering is weakly nonlinear in that tides, to the first approximation, satisfy the linearized equations, and the terms quadratic in tidal amplitude (buoyancy flux in our case) drive the mean flow of the next order. The formulation that relates the mean circulation to the tides is presented in Section 2, and the mean flows driven by the barotropic and baroclinic tide are considered separately in Sections 3 and 4. The model results are compared with observations over Georges Bank in Section 5.

2. THE THEORY

Let us consider an idealized shelf geometry that varies only in one spatial coordinate (y), as schematically shown in Fig. 1. Assuming a spatial homogeneity in x of all the field variables and an ocean that is vertically stratified, the buoyancy balance in a Boussinesq, adiabatic fluid is governed by the equation

$$\rho_t + v\rho_y + w\rho_z - \frac{N^2}{g} w = 0, \tag{2.1}$$

where ρ is the density perturbation of the reference state, v and w are the velocity components along the y and z axis, respectively, g is the gravitational acceleration, and N is the Brunt-Väisälä frequency, assumed to be a function of z only. In accordance with the common usage, subscripts are used throughout this paper to indicate partial derivatives. For an imcompressible fluid, the mass continuity states that

$$v_y + w_z = 0, \tag{2.2}$$

which, when combined with (2.1), leads to

$$\rho_t + (v\rho)_y + (w\rho)_z - \frac{N^2}{g} w = 0, \tag{2.3}$$

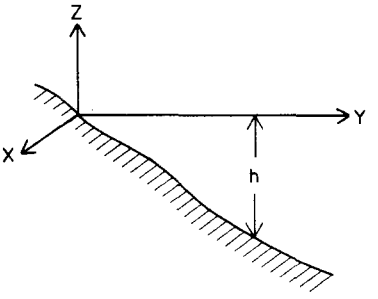

Fig. 1. A schematic of the model geometry.

Assuming that the tides satisfy the linearized equation

$$\rho_t - \frac{N^2}{g} w = 0, \tag{2.4}$$

then the mean buoyancy balance, averaged over the tidal period (denoted by an overbar), satisfies the next order equation

$$(\overline{v\rho})_y + (\overline{w\rho})_z = \frac{N^2}{g} \bar{w}. \tag{2.5}$$

Since w and ρ are in quadrature according to (2.4), the vertical buoyancy flux vanishes, and the equation (2.5) reduces to

$$(\overline{v\rho})_y = \frac{N^2}{g} \bar{w}, \tag{2.6}$$

i.e. only the cross-shelf buoyancy flux contributes to the mean vertical motion.

Take the time mean of (2.2) yields

$$\bar{v}_y + \bar{w}_z = 0, \tag{2.7}$$

from which a mean stream function ($\bar{\psi}$) can be defined

$$\bar{v} = -\bar{\psi}_z, \tag{2.8}$$

$$\bar{w} = \bar{\psi}_y. \tag{2.9}$$

Combining (2.6) and (2.9), and integrating in y, yields

$$\bar{\psi} = \frac{g}{N^2} \overline{v\rho} + F(z), \tag{2.10}$$

where F is an arbitrary function of z that can be further specified as follows: along a rigid bottom, the kinematic boundary condition dictates that v and w be 180° out of phase and, on account of the fact that w and ρ are in quadrature, $\overline{v\rho}$ vanishes. Since $\bar{\psi}$ also vanishes at the bottom, (2.10) implies that F must vanish at any z that intersects the sloping bottom. For a shelf geometry in which the bottom shoals to the surface, F must then vanish identically and (2.10) reduces to

$$\bar{\psi} = \frac{g}{N^2} \overline{v\rho}. \tag{2.11}$$

For a submarine bank, (2.11) applies only below the sill depth, as any $\bar{v}$ (but constant in y) can be added to the mean field above the sill depth without violating either the buoyancy balance or the kinematic boundary constraints. Other physical considerations beyond the scope of the present paper, such as symmetry requirements or momentum balance, are needed to remove this degeneracy.

For a uniformly stratified fluid, (2.11) thus implies that the mean stream lines coincide with the contours of the lateral buoyancy flux. With a time dependence of $e^{-i\sigma t}$ for the tide

where σ is the tidal frequency, (2.11) becomes, upon substitution from (2.4)

$$\bar{\psi} = \frac{1}{\sigma} \overline{v \cdot iw}. \tag{2.12}$$

Using this formula, the mean stream function can be calculated straightforwardly given any tidal field.

It is interesting to notice that (2.12) does not contain the stratification parameter; i.e. for a given tidal field, the mean stream function is independent of the stratification. Physically, this is because a varying stratification, although changes the magnitude of the buoyancy flux for given tidal flows, also inhibits to a different degree the mean vertical motion. The two effects exactly cancel out and the mean motion remains unchanged. The role of the stratification, at least in this context, appears to be somewhat similar to that of a linear bottom drag in many of the wave-mean flow theories (e.g. Ou and Bennett, 1979). In these latter cases, the friction causes the necessary phase shift among the oscillatory components to facilitate a non-zero momentum or vorticity transfer from the oscillatory to the mean motion, but on the other hand, also provides the bottom stress or torque to balance this input. Since the strength of both the source and sink of the mean balance is proportional to the frictional coefficient, the resulting mean flow is not very sensitive to the magnitude of this coefficient. But as in these latter cases, it is absolutely essential to include stratification in the model, without which the buoyancy balance cannot be formulated and the mean transverse flow becomes indeterministic. The stratification however does enter (2.12) indirectly by modifying the tidal field, as will be seen later in our discussion of the baroclinic tide.

We should emphasize that the mean field given by (2.12) is the Eulerian mean and does not necessarily transport any mean property. In fact, it is seen that the Longuet-Higgins' (1969) expression for the Stokes drift, $v_s = \partial_z (\overline{v \int w dt})$, gives a mean stream function that is equal but opposite in sign to (2.12). Since the Lagrangian mean is the sum of the Eulerian mean and the Stokes drift, it must then vanish. Physically, as discussed by Wunsch (1971), fluid particles can only drift along isopycnals in an adiabatic fluid, and in the case when the isopycnals intersect the sloping bottom, the Lagrangian mean velocity must vanish identically.

Since the tides are linear, it is conceptually useful to decompose the tides into the barotropic and baroclinic component and examine the mean flow driven by the two components separately. The decomposition is physically realizable only over a gentle topography that is relatively flat compared with the characteristics of the internal tide. Since for a semi-diurnal tide at mid-latitude, the latter has a typical slope of the order of 10^{-2} or greater, the above condition is generally satisfied over continental shelves. In the next two sections, we will examine the mean flow driven by both the barotropic and baroclinic tide.

3. BAROTROPIC TIDES

If the surface displacement is small compared with the water depth change over the distance of one tidal excursion, the surface can be treated as rigid (Loder, 1980). For a bottom slope of 10^{-3} as is typical of a continental shelf and a tidal excursion of several tens of kilometers, the latter is a few tens of meters. Even in regions closer to shore where the

surface cannot be treated as rigid, the mean flow generated by the free surface might still be negligible. A free surface allows the generation of the Stokes drift which, according to the argument put forth earlier, is balanced by an opposing Eulerian flow of equal magnitude. The Stokes drift has a magnitude of the order of v^2/c_p (LONGUET-HIGGINS, 1969), where v is the tidal amplitude and c_p is the phase speed of surface gravity waves. The magnitude of the mean flow relative to the tidal flow is thus given by the ratio v/c_p which is generally negligible. But we caution that in the nearshore zone where the free surface displacement becomes comparable to the water depth, tides can no longer be considered linear and the present theory breaks down.

With the above qualifications, rigid lid approximation will be used in the following discussions. For simplicity, we nondimensionalize (y,z) by some proper scales (L,H) and velocities (v,w) by the scales $Q/H(1, H/L)$, where Q is the amplitude of the volume transport per unit alongshelf distance, a constant in y under the rigid lid approximation. For an inviscid fluid, the tidal amplitudes are given by

$$v = 1/h, \tag{3.1}$$

and

$$w = zh_y/h^2. \tag{3.2}$$

Since v and w are 180° out of phase, $\tilde{\psi}$ vanishes according to (2.12); the barotropic tide therefore does not generate any buoyancy flux or mean transverse circulation in the inviscid limit. To incorporate the next order correction due to friction, let us consider a momentum balance of the form

$$v_t = -p_y + Ev_{zz}, \tag{3.3}$$

where

$$E \equiv 2\nu/(\sigma H^2), \tag{3.4}$$

with ν being the coefficient of kinematic eddy viscosity. For simplicity, we have temporarily left out the Coriolis term, the inclusion of which will be discussed later (Section 3.3). With the boundary conditions that

$$v = 0 \text{ at } z = -h, \tag{3.5}$$

and

$$v_z = 0 \text{ at } z = 0, \tag{3.6}$$

the vertical structure of the flow can be determined. Subject to the further constraint that

$$\int_{-h}^{0} v\,dz = 1, \tag{3.7}$$

the solution is given by

$$v = \tilde{v}\,(1 - \cosh mz/\cosh mh), \tag{3.8}$$

where

$$\tilde{v} = -\frac{i}{\sigma} p_y = \frac{1}{h}\,(1 - \tanh mh/mh)^{-1},$$

and

$$m = (1 - i)/\sqrt{E}.$$

The accompanying tidal fields are given by

$$\psi = -h\bar{v}\left[1 + \frac{z}{h} - \frac{\tanh mh}{mh}\left(1 + \frac{\sinh mz}{\sinh mh}\right)\right], \tag{3.9}$$

and

$$w = hh_y\,\bar{v}^2 \tanh^2 mh \left(\frac{z}{h} - \frac{\sinh mz}{\sinh mh}\right). \tag{3.10}$$

Since the topography enters the problem only parametrically, the above solution applies to a general topography, but for the purpose of illustration, we will consider a wedge geometry, which also allows for a more direct comparison with the solutions in later sections. In Figs 2 to 4, we have plotted the tidal amplitude (solid lines) and phase (dashed

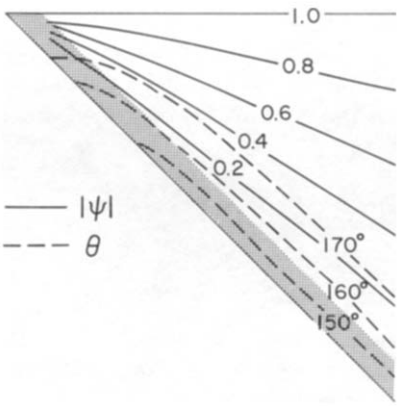

Fig. 2. The amplitude (solid lines) and phase (dashed lines) of the stream function for a barotropic tide in a wedge, with $E = 0.01$. The shaded area represents the Stokes layer.

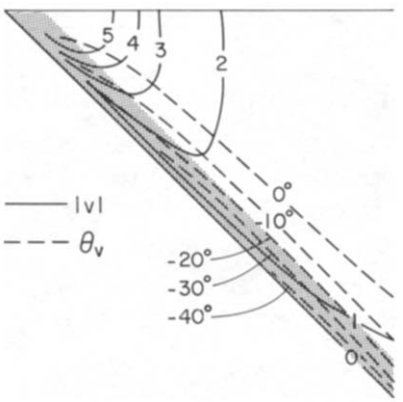

Fig. 3. Same as Fig. 2, but for the velocity component v.

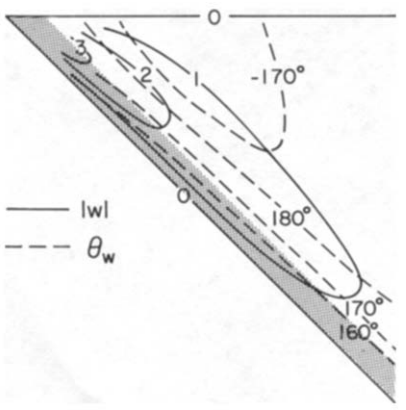

Fig. 4. Same as Fig. 2, but for the velocity component w.

lines) for the case $E = 0.01$. The scales have been chosen so that the wedge has a unit slope (i.e. $H/L = \gamma$, γ being the original wedge slope) and that the seaward boundary has a unit depth. The shaded area represents the frictional boundary layer, given by the Stokes scale $E^{1/2}$.

Without friction, v would be vertically uniform and w increases linearly toward the bottom. Friction, besides reducing both amplitudes to zero at the bottom, also induces an upward phase propagation. This feature can be understood by examining (3.3) more closely. If we write the solution (3.8) as the sum of the depth-independent component (i.e. $\bar{v}$) and a frictional correction (v'), then v' satisfies the diffusive equation [i.e. (3.3) without the pressure gradient term] with a non-homogeneous boundary condition at the bottom ($v' = -\bar{v}$). The signal thus propagates upward, much like the heat waves travelling through a conducting rod from an oscillatory heat source applied at one surface (MORSE and FESHBACH, 1953, p. 1580).

In the far field where the boundary layer is thin relative to the water depth, the only relevant scale is the Stokes depth and, as expected, the phase lines are parallel to the bottom. But as the boundary layer thickness becomes comparable to the water depth near the apex, significant distortion of the phase lines occurs. It will be seen more clearly from the asymptotic solution of the next section that the vertical phase differential is reduced as the apex is approached, and the reduction is more rapid for the w component due perhaps to the stronger constraint imposed by the rigid surface. On account of the exact out of phase relation between w and v at the bottom, w thus lags v by $< 180°$ higher up in the water column. Since w leads ρ by 90° for an adiabatic fluid, the lateral buoyancy flux is thus directed down the slope ($\overline{v\rho} < 0$) or, according to (2.11), a negative $\bar{\psi}$.

We have plotted in Fig. 5 the mean stream function $\bar{\psi}$ which has been scaled according to $[\bar{\psi}] = \varepsilon[\psi]$, where

$$\varepsilon \equiv \frac{[v]}{\sigma L} = \frac{[w]}{\sigma H} \tag{3.11}$$

is the ratio of the tidal excursion to the horizontal scale, or the ratio of the vertical displacement scale to the depth scale (the inverse of which has sometimes been called Strouhal's number). The bracket enclosing the variable is used throughout this paper to

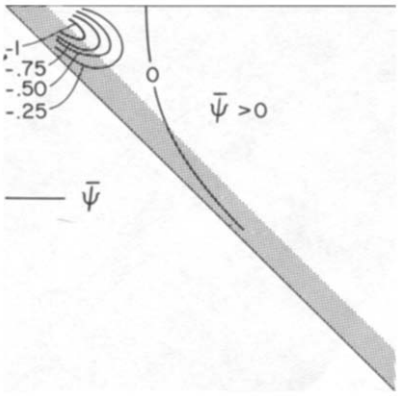

Fig. 5. The mean stream function driven by the tidal fields shown in Figs 2 to 4.

indicate the scales. It is seen that $\bar{\psi}$ is slightly positive offshore when the frictional boundary layer is thin relative to the water depth, but is significant only near the apex where the Stokes scale is comparable to the water depth and there the mean flow is characterized by a single-cell circulation with offshore flow near the bottom. To examine the solution more closely, let us consider its asymptotic limits in the near and far fields in the next two subsections.

3.1 *The near field* ($E^{1/2} \gg h$)

Expanding the solutions (3.8) and (3.10) in terms of the small parameter mh, we obtain

$$v \approx \frac{3}{2h}\left(1-\frac{z^2}{h^2}\right)\left[1-\frac{1}{60}(mh)^2\left(1-5\frac{z^2}{h^2}\right)\right], \tag{3.12}$$

and

$$w \approx \frac{3}{2h}\cdot\frac{z}{h}\left(1-\frac{z^2}{h^2}\right)\left[1+\frac{1}{60}(mh)^2\left(1+3\frac{z^2}{h^2}\right)\right]. \tag{3.13}$$

To the lowest order, the vertical profiles of the tidal velocities thus approach a universal form that depends only on the relative depth within the water column (z/h), and there is no frictional correction on the phase. At a fixed z/h, the amplitudes increase toward the apex as h^{-1}. Substituting the above solution into (2.12) yields

$$\bar{\psi} \approx \frac{3}{40E}\left(\frac{z}{h}\right)\left(1-\frac{z^2}{h^2}\right)^3. \tag{3.14}$$

It is seen that at a fixed z/h, $\bar{\psi}$ is constant in y despite the increase of the tidal amplitudes as the apex is approached. This is because the friction-induced phase shift that causes the net buoyancy flux is contained in the higher order terms of $(mh)^2$ and thus is rapidly diminishing toward the apex. Using (2.8) and (3.14), the mean cross-wedge flow $\bar{v}$ can be

derived,

$$\bar{v} = -\frac{3}{40E} \cdot \frac{1}{h}\left(1 - \frac{z^2}{h^2}\right)^2 \left(1 - 7\frac{z^2}{h^2}\right), \tag{3.15}$$

which varies as h^{-1} at fixed z/h, the same rate as that of the tidal velocities. If we rescale $\bar{v}$ by

$$[\bar{v}] = \frac{\varepsilon}{E}[v], \tag{3.16}$$

then the factor E drops out of the expression (3.15), which is plotted in Fig. 6, together with the tidal velocities, as a function of the relative water depth z/h.

Besides the general properties previously described, the figure shows that the magnitude of the mean cross-wedge flow can reach a few percentage of the maximum tidal velocity in the dimensionless unit. To estimate its dimensional magnitude, we rewrite the scaling factor (ε/E) in (3.16) as $Q\gamma/2\nu$, using the definitions of ε (equation 3.11) and E (equation 3.4). This scaling factor obviously varies greatly over different tidal regimes. For a realistic tidal regime with, say, $Q \approx 2 \times 10^5$ cm^2 s^{-1} (corresponding to a tidal flow of 20 cm s^{-1} over a 100 m water depth), γ (bottom slope) $\approx 10^{-3}$, ν (coefficient of kinematic eddy viscosity) $\approx 10^2$ cm^2 s^{-1}, it has the value of one, and can be considerably greater for stronger tides or steeper bottom slopes. The mean cross-wedge flow thus can reach a few percentage or even a significant fraction of the tidal velocities when friction dominates the water column. Notice that the scaling factor is inversely proportional to ν. For greater ν, although the asymptotic solution is valid to greater water depths, the mean flow actually decreases due to the diminishing phase shift in the tidal components.

3.2 *The far field* ($E^{1/2} \ll h$)

To examine the solution in the far field where the frictional boundary layer is thin relative to the water depth, we expand the solution (3.8), (3.9) and (3.10) in terms of the

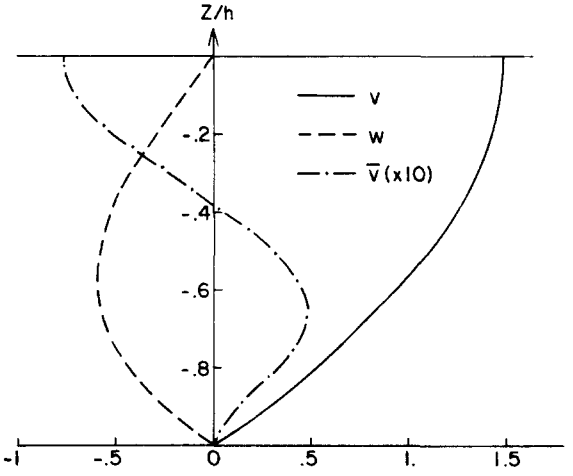

Fig. 6. The velocities (multiplied by h) in the near field.

small parameter $(mh)^{-1}$, which yields

$$\psi \approx -\left(1 + \frac{1}{mh}\right)\left[\zeta - \frac{1}{mh}\left(1 - e^{-mh\zeta}\right)\right], \tag{3.17}$$

$$v \approx \frac{1}{h}\left(1 + \frac{1}{mh}\right)(1 - e^{-mh\zeta}), \tag{3.18}$$

$$w \approx \frac{1}{h}\left(1 + \frac{2}{mh}\right)(\zeta - 1 + e^{-mh\zeta}), \tag{3.19}$$

where $\zeta = 1 + z/h$ is the distance above the bottom expressed in terms of the fraction of the water depth. Let η $(\equiv h\zeta/\sqrt{E})$ be the same distance expressed in terms of the Stokes scale, then to the lowest order, the amplitude and phase of the tidal velocity (3.18) become

$$|v| = \frac{1}{h}[1 - 2e^{-\eta}\cos\eta + e^{-2\eta}]^{1/2}, \tag{3.20}$$

$$\theta_v = \tan^{-1}[(-e^{-\eta}\sin\eta)/(1-e^{-\eta}\cos\eta)], \tag{3.21}$$

and the mean cross-wedge flow, obtained from substituting the tidal velocities (3.18) and (3.19) into (2.12) and (2.8), is given by

$$\bar{v} = -\frac{1}{2h^3}e^{-\eta}[\eta\sin\eta + (1-\eta)\cos\eta - e^{-\eta}]. \tag{3.22}$$

Notice that at a fixed η, $|v|$ decreases offshore as h^{-1}, while $\bar{v}$ decreases at a much faster rate of h^{-3}. Setting $h = 1$, we have plotted both the tidal and mean cross-wedge flow in Fig. 7. The friction correction to the tidal flow, as expected, is confined to the boundary layer

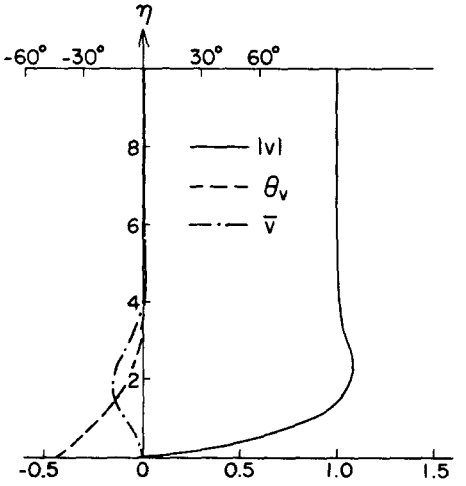

Fig. 7. The asymptotic solution in the far field. The ordinate is the distance above the bottom expressed in terms of the Stokes scale.

where an upward phase propagation is apparent. The total phase lag between the bottom and interior is 45°, as can be derived from (3.21). The mean cross-wedge flow is significant only within the bottom boundary layer where it is directed primarily onshore. Its magnitude reaches about 20% of the tidal velocity in the dimensionless unit. Since the scaling factor ε is generally one or two orders of magnitude smaller than unity in the far field [for a typical tidal regime of, say, $[v] \approx 20$ cm s^{-1}, $\sigma \approx 2 \times 10^{-4}$ s^{-1}, and $L \approx 100$ km, ε is 10^{-2}], the mean cross-wedge flow there is generally negligible.

3.3 *Coriolis effect*

The solution (3.8) can be extended to the case when there is rotation (SVERDRUP, 1926; MOFJELD, 1980). The most notable effect of the rotation is the introduction of two instead of one frictional scale. With E now denoting the Ekman number and the tidal frequency scaled by the inertial frequency, the two frictional depths (scaled by the Ekman depth) are given by $(1 - \sigma)^{-1/2}$ and $(1 + \sigma)^{-1/2}$. We have plotted in Fig. 8 the frictional depths l as a function of the tidal frequency σ. It is seen that the thickness of the inner boundary layer is rather constant, and that there is a significant split of the two scales only near the inertial latitude which, for a semi-diurnal tide, is located near the poles. In Figs 9 and 10 we have plotted the mean stream function (solid lines) and the phase lines of the tidal stream function (dashed lines) for the two cases of $\sigma = 1.5$ and $\sigma = 1.1$ with $E = 0.01$. The inner and outer boundary layer are shaded for visual reference. When the two frictional scales are comparable (as in Fig. 9), the result is qualitatively similar to the nonrotating case (Figs 2 and 5), but when there is a significant split of the two frictional scales (as in Fig. 10), there is a region within the outer boundary layer that simulates the far field with respect to the inner boundary layer, as can be seen by the upward bending of the phase lines near the apex just above the inner boundary layer. Drawing comparison with the nonrotating solution, this results in a region of positive stream function embedded in regions of negative stream function caused by the frictional effect of the two boundary layers. Despite this complication, the mean flow is still significant only in the corner region where the water depth is comparable to the thickness of the inner boundary layer and where the asymptotic solution discussed in Section 3.1 remains valid.

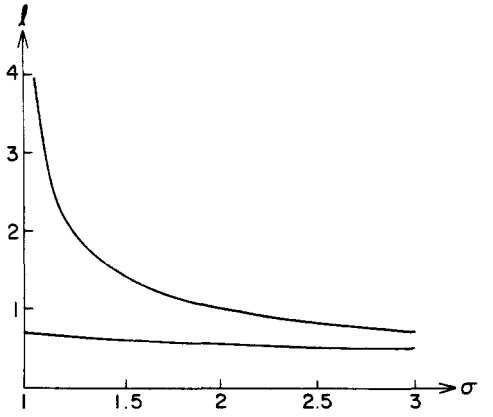

Fig. 8. The frictional depths l (scaled by the Ekman layer depth) as a function of the tidal frequency.

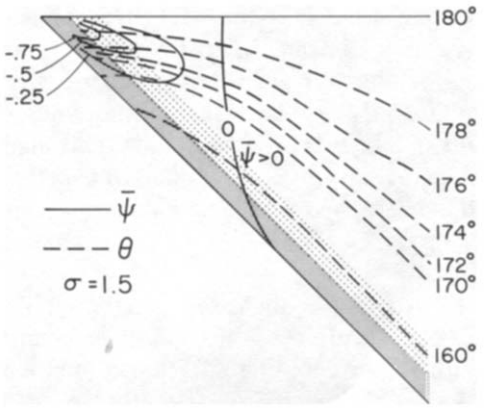

Fig. 9. The mean stream function (solid lines) and the phase lines of the tidal stream function (dashed lines) for the case of $\sigma = 1.5$ with $E = 0.01$. The shaded areas represent the inner and outer boundary layers.

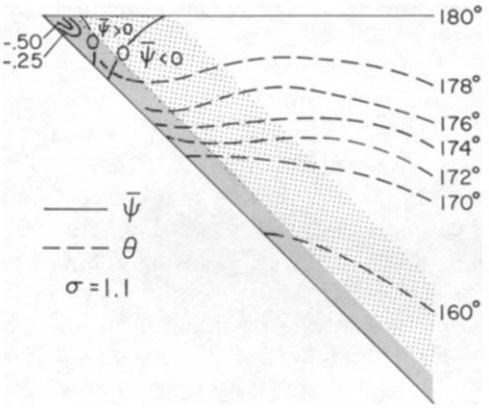

Fig. 10. Same as Fig. 9, but for a tidal frequency $\sigma = 1.1$.

3.4 *Summary*

We summarize below the main results for the barotropic tide:

(1) Under the model idealization, the barotropic tide does not generate any buoyancy flux or mean transverse circulation in the inviscid limit.

(2) Friction causes an upward phase propagation in the tidal fields. The relative phase shift among different tidal components results in a non-zero buoyancy flux that drives the mean flow.

(3) The mean flow is significant only in the near field where friction dominates the water column and is characterized by a single-cell circulation with offshore flow near the bottom.

(4) In the near field, at any fixed relative depth of the water column, the mean flow varies as $1/h$, the same rate as the tidal velocities, and its magnitude can reach a few percentage or a significant fraction of the tidal velocities.

(5) As we move offshore out of the near field, the mean flow diminishes at a faster rate than the tidal flow. And when the boundary layer is thin relative to the water column, the mean flow, significant only in the boundary layer, varies as h^{-3} at any fixed distance above the bottom. Its magnitude is generally negligible compared with tidal flows.

(6) Coriolis force introduces two frictional scales, but the mean flow is significant only where the thickness of the inner boundary layer is comparable to the water depth and the circulation there is qualitatively similar to that in the nonrotating case.

4. BAROCLINIC TIDES

WUNSCH (1971) has calculated the mean transverse flow driven by internal waves in a wedge filled with uniformly stratified fluid. Although his solution is for a nonrotating case, the only modification that needs to be made to accommodate the rotation is to replace his expression of c (the slope of the characteristics) by $[(\sigma^2 - f^2)/(N^2 - \sigma^2)]^{1/2}$. So the only new elements here are the physical discussions on the buoyance flux and some quantitative statements about the magnitude of these mean flows. Wunsch's solution is for inviscid modes in a subcritical wedge which can be somewhat justified in the tidal problem by the argument that friction correction generally confines to the bottom boundary layer and that for a semi-diurnal tide, a typical shelf is almost always subcritical except in polar regions.

The mean flow simply changes sign between the up- and down-slope propagating modes, but in anticipation of later comparison with observation, we will further restrict our discussion to the former ones for the following reasons: the internal tides observed on the shelf are primarily generated offshore—due to the interaction of the surface tide with steep topography—and propagate onto the shelf. Theoretical studies (PRINSENBERG *et al.*, 1974) have shown that a combination of gentle slope and friction is very efficient in absorbing the incoming waves or damping out the reflected waves. And this is further corroborated by oceanic observations that generally show a shoreward propagation for the internal tides on the shelf (WUNSCH, 1975).

Since an infinite wedge has no intrinsic length scales, the only independent variable is the relative depth within the water column ($z' \equiv z/h$), and the only external parameter is the ratio of the bottom slope to the slope of the characteristics ($\gamma' \equiv \gamma/c$). Wunsch's solution for the n^{th} mode (adapted to our notation) is given by

$$\psi = \sin\Gamma \cdot \exp(i\theta), \tag{4.1}$$

where

$$\Gamma = \frac{q}{2} \ln \frac{1 - \gamma' z'}{1 + \gamma' z'},$$

$$\theta = \frac{q}{2}(1 - \gamma'^2 z'^2) \ln (h^2 \gamma'^{-2}),$$

with

$$q = 2n\pi / \ln\left(\frac{1 + \gamma'}{1 - \gamma'}\right).$$

If we set the horizontal scale L to be H/c, the tidal velocities are given by (setting h to 1)

$$v = \frac{1}{n\pi} \cdot \frac{q\gamma'}{1 - \gamma'^2 z'^2} (\cos^2 \Gamma + \gamma'^2 z'^2 \sin^2 \Gamma)^{1/2} \exp(i\theta_v), \tag{4.2}$$

$$w = \frac{1}{n\pi} \cdot \frac{q\gamma'}{1 - \gamma'^2 z'^2} (\gamma'^2 z'^2 \cos^2 \Gamma + \sin^2 \Gamma)^{1/2} \exp(i\theta_w), \tag{4.3}$$

where

$$\theta_v = \theta - \tan^{-1}(\gamma' z' \tan \Gamma),$$

and

$$\theta_w = \theta - \tan^{-1}(\tan \Gamma / \gamma' z').$$

The velocities have been normalized such that their maximum amplitude is 1 when the bottom is flat. Substituting the solution (4.2) and (4.3) into (2.12), one obtains

$$\bar{\psi} = \frac{1}{4n^2\pi^2} \cdot \frac{q^2\gamma'^2}{1 - \gamma'^2 z'^2} \sin 2\Gamma,$$

accompanied by a mean cross-wedge flow

$$\bar{v} = \frac{1}{2n^2\pi^2} \cdot \frac{q^3\gamma'^3}{(1 - \gamma'^2 z'^2)^2} (\cos 2\Gamma - \gamma' z' \sin 2\Gamma).$$

We have plotted in Figs 11 to 14 both the tidal amplitudes and the mean field for the first mode ($n = 1$) and for three different values of the relative bottom slope γ'. It is seen that the buoyancy flux (which is proportional to the mean stream function) is offshore in the lower level, but changes sign above some mid-depth. This can be explained by considering an instantaneous tidal field sketched in Fig. 15 where an upward motion is accompanied by the convergence of the lateral velocity in the lower level (and the divergence of the lateral velocity in the upper level). This upward motion tends to increase the density of the water column, which attains a maximum a quarter cycle later, by which time, because of the shoreward propagation, the lateral flow in the lower level is onshore (the dashed arrow). Similarly, during the next half cycle, the minimum density concurs with an offshore flow in the lower layer. This net correlation between the lateral velocity and the density anomaly

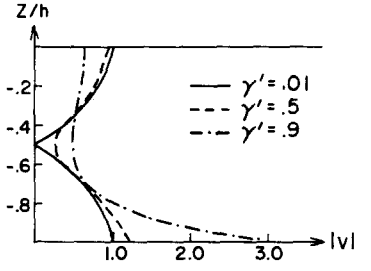

Fig. 11. Velocity amplitude $|v|$ of the first baroclinic mode ($n = 1$) for three different values of γ' (the relative bottom slope with respect to the slope of the characteristics).

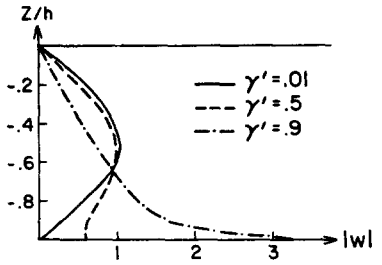

Fig. 12. Same as Fig. 11, but for the velocity amplitude $|w|$.

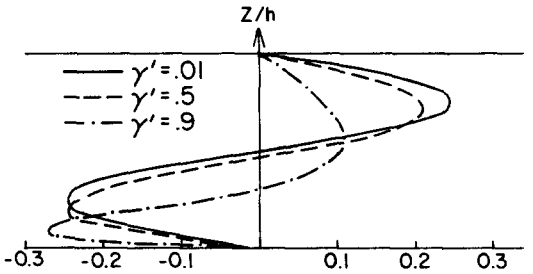

Fig. 13. Same as Fig. 11, but for the mean stream function $\bar{\psi}$.

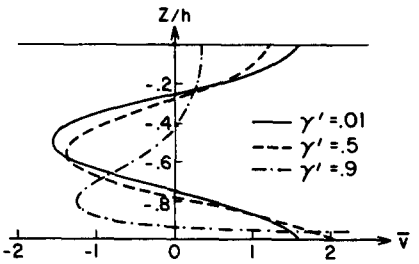

Fig. 14. Same as Fig. 11, but for the mean cross-wedge velocity $\bar{v}$.

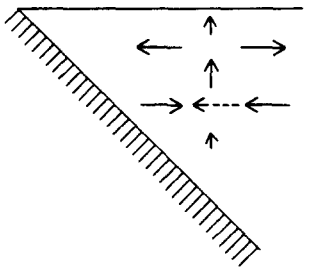

Fig. 15. A schematic drawing explaining the tidal-induced buoyancy flux.

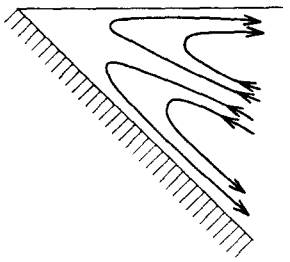

Fig. 16. A schematic drawing of the mean stream function induced by the first-mode baroclinic tide.

over a tidal period thus results in an offshore buoyancy flux in the lower level. In the upper level where the lateral velocity reverses, the buoyancy flux changes sign and is directed onshore. Since the boundary flux vanishes along the sloping bottom, the buoyancy deficit (surplus) in the lower (upper) level induced by the tidal flux must be accompanied by a mean downward (upward) motion in the lower (upper) level. Through mass continuity, the mean circulation thus consists of a pair of half-open (on the seaward side), counter-rotating cells with shoreward flow at mid-depth and offshore flow both above and below, as schematically shown in Fig. 16. For higher modes, the number of pairs increases, being equal to the mode number, but, as clear from the above argument, the flow direction remains offshore near the top and bottom surface.

It is also interesting to note that the mean flow is not very sensitive to the variation of the external parameter γ' except very near the critical point (i.e. $\gamma' = 1$) when it becomes infinite near the bottom where the frictional effect must become important. Comparing Figs 11 and 14, it is seen that the magnitude of the mean flow is of the same order to that of the tidal flow in the dimensionless unit. Since the scaling factor ε (as defined in equation 3.11) is the ratio of the vertical displacement scale to the water depth which can be a significant fraction of one for the internal tide, so can the magnitude of the mean cross-wedge flow relative to the tidal flows. The linear theory breaks down when ε approaches 1.

5. APPLICATIONS

Although the mean cross-wedge flow driven by the barotropic tide or the baroclinic tide of different mode number has very different spatial structure, it always points offshore near the bottom. Furthermore, its magnitude can reach a significant fraction of the barotropic tidal velocities or a large fraction of the baroclinic tidal velocities in realistic tidal regimes. Although the model is highly idealized for mathematical simplicity, the physical mechanism we have presented is sufficiently general that the above conclusions should apply to less idealized geophysical environments. Is there any observational evidence for this tidally induced transverse flow? For this, we shall examine the published data on Georges Bank which is known for strong tides that typically reach an amplitude of several tens of cm s^{-1}.

BUTMAN *et al.* (1982) have recently compiled four years (1975 to 1979) of current meter data to construct a mean Eulerian flow field over the Bank (their Fig. 4). The most noticeable feature is the anticyclonic circulation around the Bank, but a closer examination of the mean flow also reveals that, with perhaps two or three possible exceptions out of a total of 15 mooring sites around the Bank, the mean flow near the bottom always

points off the Bank, and the off-bank flow is particularly strong for mooring sites located over steeper slopes, consistent with the model predictions.

A good evidence that links the off-bank flow to the tides can be found in MAGNELL *et al.* (1980). From analyzing the current meter data over the northern slope of the Bank, they found a significant correlation (0.74) between the low-frequency off-bank flow and the tidal modulation for the near-bottom measurements. Furthermore, neither variable is coherent with the local wind, thus discounting the likelihood that both are simply responding to the same wind and hence appear to be correlated. Their analysis strongly suggests a tidal origin for the low-frequency variation of the off-bank flow and the flow direction agrees with that predicted by the model. The correlation between the low-frequency off-bank flow and the tidal modulation rapidly drops to 0.04 at mid-depth (still below the sill depth), again consistent with the model results that the mean flow direction there is less definite due to contributions from different tidal components.

As discussed before, the Eulerian mean does not transport any property in this simplified model because the Eulerian flux is exactly cancelled out by the tidal flux. The Eulerian mean that we have calculated however is important in other respects. Under the action of the Coriolis force, it can drive a mean flow along isobaths. Although when vertically integrated, the net effect vanishes under the rigid lid assumption, it can play a role in determining the vertical structure of the mean along-isobath flow. The observations of BUTMAN *et al.* (1982) and MAGNELL *et al.* (1980) show a mean off-bank flow of the order of a few cm s^{-1} which, if not impeded by friction, can accelerate a mean along-isobath flow to the same magnitude within an inertial period.

Acknowledgements—This work was initiated and the bulk of it carried out during H. W. Ou's visit to the University of Utrecht in The Netherlands. The visit was partly funded by the Directorat General for Science Policy of the Department of Education and Science of The Netherlands. He wants to acknowledge the hospitality and the stimulating environment provided by the University. H. W. Ou's research was also supported by the National Science Foundation under Grant OCE81-17579 and the Department of Energy under Grant DE-AC02-76EV02185FX Lamont-Doherty Geological Observatory Contribution No. 3852.

REFERENCES

BRETHERTON F. P. (1969) On the mean motion induced by internal gravity waves. *Journal of Fluid Mechanics*, **36**, 785–803.

BUTMAN B., R. C. BEARDSLEY, B. MAGNELL, D. FRYE, J. A. VERMERSCH, R. SCHLITZ, R. LIMEBURNER, W. R. WRIGHT and M. A. NOBLE (1982) Recent observations of the mean circulation on Georges Bank. *Journal of Physical Oceanography*, **12**, 569–591.

CHARNEY J. G. and P. G. DRAZIN (1961) Propagation of planetary-scale disturbances from the lower into the upper atmosphere. *Journal of Geophysical Research*, **66**, 83–109.

LODER J. W. (1980) Topographic rectification of tidal currents on the sides of Georges Bank. *Journal of Physical Oceanography*, **10**, 1399–1416.

LONGUET-HIGGINS M. S. (1969) On the transport of mass by time-varying ocean currents. *Deep-Sea Research*, **16**, 431–447.

MAGNELL B. A., S. L. SPIEGEL, R. I. SCARLET and J. B. ANDREWS (1980) The relationship of tidal and low-frequency currents on the north slope of Georges Bank. *Journal of Physical Oceanography*, **10**, 1200–1212.

MCINTYRE M. E. (1977) Wave transport in stratified, rotating fluids. In: *Lecture notes in physics*, Vol. 71, E. A. SPIEGEL and J. P. ZAHN, editors, Springer-Verlag, New York, pp. 290–314.

MOFJELD H. O. (1980) Effects of vertical viscosity on Kelvin waves. *Journal of Physical Oceanography*, **10**, 1039–1050.

MORSE P. M. and H. FESHBACH (1953) *Methods of theoretical physics*, 2 parts, McGraw-Hill, New York, 1978 pp.

OU H. W. and J. R. BENNETT (1979) A theory of the mean flow driven by long internal waves in a rotating basin, with application to lake Kinneret. *Journal of Physical Oceanography*, **9**, 1112–1125.

PRINSENBERG S. J., W. L. WILMOT and M. RATTRAY, JR. (1974) Generation and dissipation of coastal internal tides. *Deep-Sea Research*, **21**, 263–281.

SVERDRUP H. U. (1926) Dynamics of tides on the North Siberian Shelf. *Geofysiske Publikasjoner*, 4, No. 5.
WUNSCH C. (1971) Note on some Reynolds stress effects of internal waves on slopes. *Deep-Sea Research*, **18**, 583–591.
WUNSCH C. (1975) Internal tides in the ocean. *Reviews of Geophysics and Space Physics*, **13**, 167–182.
ZIMMERMAN J. T. F. (1980) Vorticity transfer by tidal current over an irregular topography. *Journal of Marine Research*, **78**, 601–630.